Plasma Nitriding of CrMoV Steel for the Enhancement of Hardness and Corrosion Resistance

D. Bhadraiah[1] · Corinne Nouveau[2] · K. Ram Mohan Rao[1]

Received: 7 August 2021 / Accepted: 11 September 2021 / Published online: 12 October 2021

Abstract In the plasma ionic environment of nitrogen and hydrogen at 4:1 ratio, nitriding had been realized in the plasma laboratory. Nitriding of steel samples was followed at the lower temperature of 450 °C and also at the higher temperature of 550 °C while the sample was biased at the fixed − 250 V. Steel nitrided at 550 °C had shown a significantly enhanced resistance to corrosion in comparison to that of steel nitrided at 450 °C. X-ray diffraction studies of nitrided steels had shown the presence of nitrides of iron (FexN). Scanning electron microscopic and the electron dispersive spectroscopic analyses (SEM + EDS) of the cross section of the nitrided steels had shown the nitrided layer and the elemental distribution from top to the core. Following structural analysis, microhardness and the potentiodynamic polarization tests were performed. A significant improvement in hardness (∼ 1180 Hv) and the case depth ∼ 150 µm was obtained after nitriding at the higher temperature. Corrosion resistance was also found to be significantly improved. These achievements might be attributed to the presence of FexN, CrN phases and also to the nitrogen solid solution.

Keywords Corrosion · Polarization · Surface hardness · Microstructure · Steel · X-ray diffraction

✉ K. Ram Mohan Rao
rammohanrao.k@gmail.com

[1] Department of Chemistry, GITAM Institute of Science, GITAM University, Rushikonda, Gandhinagar, Visakhapatnam 530045, India

[2] Laboratoire Bourguignon Des Matériaux Et Procédés (LaboMaP), Arts et Métiers Paris Tech de Cluny, Rue Porte de Paris, 71250 Cluny, France

1 Introduction

High nitrogen alloys as the new class of materials had been the interest of the researchers and industrial sectors for its novel properties [1–10]. Like carbon in Fe–C alloys, nitrogen is also a good candidate for achieving the similar properties as shown by carbon. This is how it can cutoff the carbon content in the Fe–C alloy and give rise to Fe–N alloys and thus satisfy the present day's need of human survival in the less carbon environment [11]. N is the next to C in the periodic table with atomic number 7 and 6, respectively. Its atomic radii are also very near to carbon atom and both are forming interstitial solid solutions. The phase diagrams of Fe–N and Fe–C show the similar characteristics at eutectoid transformation point and show the stability of some phases viz. ferrite, pearlite, austenite and martensite [11]. It has been realized that the Fe–N alloys have significant improvement in corrosion resistance and mechanical properties. As compared to carbon inclusion, the nitrogen inclusion in the solid solution is found to be more advantageous, i.e., the interstitial solubility of N in ferrite is ∼ 0.1 wt% and ∼ 2.8 wt% in austenite leading to the greater effects on solid solution strengthening of ferrite and the austenite stability. On the other hand, a lower eutectoid temperature of 592 °C significantly saves the cost of the heat treatment [12–15].

Nitrogen as alloying element has the significant role in improving the corrosion resistance of steels such as austenitic stainless steel, duplex stainless steels [16–20]. Nitrogen in stainless steel enhances the resistance to pitting corrosion for which the following established equation is well known in terms of Pitting Resistance Equivalent Number – PREN given as follows: PREN = %Cr + 3.3 × % Mo + 16 × % N.

From mechanistic point of view N improves corrosion resistance by the formation of ammonia, anodic segregation, promoting Cr enrichment in the corrosion resisting passive film, synergistically affecting with the Cr and Mo, formation of iron nitrides with inherent property to resist corrosion and chloride repulsion theory and decreasing the point defects density [19, 21–26]. Nitrogen had been successfully incorporated in various steels by following nitriding process with the view to improve the mechanical and corrosion resistance properties. However, less is known about the effect on corrosion resistance of N incorporated martensitic stainless steel. The nitrogen solubility at atmospheric condition is too low to improve the resistance to corrosion. It may be expected that incorporation of nitrogen by ion nitriding process increases the N content in the solid solution. In this regard, plasma-assisted nitriding had been recognized as a successful method for including nitrogen in the metallic materials like steel, titanium etc. [27–36]. Though, plasma nitriding has been successfully applied for the various steels but a fewer studies have so far been made on the plasma nitriding of wood machining medium carbon martenstic stainless steel [27, 29, 33]. The surface of the tool made of this steel encounters commonly the frictional forces, and frequent jerks from the obstacles like knots inside the wood which exert high impact load, electrochemical wood juice oozing out during the wood machining from the body of the wood, and also other chemical agencies when exposed to the environment. To combat these problems causing mechanical and electrochemical degradation, surface modification of the materials is necessitated.

Hard coatings following physical or chemical vapor deposition is commonly practiced to solve the problem but the delamination of the deposited layer limits its widespread applications and reduces the longevity of the service life of the tool. Nitriding can overcome these problems by improving the surface hardness and the bringing the microstructural changes viz. dispersion of corrosion resistant and hard phases of nitrides. By inducing the compressive stress on the surface after nitriding the fatigue property can also be enhanced. The conventional nitriding offers only limited process control and is neither cost-effective nor eco-friendly. Long duration of nitriding to achieve the desirable thickness of the nitrided layer is not cost effective. In this regard, plasma nitriding had been recognized as more effective with several advantages viz. the cost-effectiveness, variable process control to achieve the desirable phases and the modified layer thickness within the short duration of the treatment time.

Nouveau et al. [27] improved the hardness of this steel and later Rao et al. [29, 33] studied the effects on corrosion resistance after plasma nitriding. The present study is concerned with the effects of high temperature nitriding on this steel. The corrosion resistance after nitriding has been the focus of this study.

2 Experimental Procedure

Medium carbon steel coupons (present steel) of $15 \times 10 \times 5$ mm^3 dimensions were cut from a bigger sheet of the steel after performing the heat treatment. The compositional analyses of the steel are summarized in Table 1 as shown below:

These sample coupons after metallographic polishing were cleaned ultrasonically in acetone to degrease and remove the deposited dirt or contaminants. The sample coupons so prepared were kept in the vacuum vessel of the plasma nitriding reactor and then evacuated by using the rotary and the diffusion pump coupling to a pressure 0.06×10^{-2} mbar. Sample coupons through the sample holder were connected to the power supply. The power supply was used to bias the sample negatively at 250 V which was required to accelerate the positively charged ions of nitrogen and hydrogen present in the plasma toward the surface of the sample. The nitriding parameters are summarized in Table 2 as below:

Ar gas was then fed into the vacuum chamber until the working pressure of $\sim$ 0.5 mbar achieved.

Following this, the plasma was triggered and bombarded on the steel surface until the desired temperature for nitriding was achieved. Ar + ions sputterred cleaned the native oxide/dirt on the surface of the steel samples. Once the desired temperature was achieved, the ion bombardment stopped and nitriding cycle initiated after feeding the nitrogen and hydrogen gas mixture (at 4:1 ratio).

Nitriding was performed at a lower temperature of 450 °C and also at the higher temperature of 550 °C with the variation in the duration of the process. Temperature was monitored carefully to maintain the fluctuation within the range of ± 5.0 °C. After the nitriding cycle, the process was stopped and the sample coupons were allowed to cool in the chamber environment. It was cooled in the nitrogen and hydrogen gas environment to avoid the risk of oxidation. After cooling, gas feeding was stopped and the vacuum pumps were switched off and finally sample coupons were taken out of the vacuum chamber.

The visual inspection of the nitrided samples by unaided eyes has shown the difference in the reflection of surface. The surface of the bare steel (A) in Fig. 1 appears bright but after nitriding turns grayish as shown in Fig. 1b which is the typical color of the nitrided steel.

Both the bare and the nitrided steel coupons were the exposed to X-ray diffraction (XRD- XRD INEL CPS 120 diffractometer θ/2θ configuration) and scanning electron microscopic analyses (SEM) to reveal the microstructure of

Table 1 Compositional analyses of the various constituents of the steel in the present studies

Elements	Cr	C	Mn	V	Si	Mo	Fe
wt%	8.0	0.5	0.5	0.5	1	1.5	Bal

Table 2 Nitriding parameters

Steel	Temp. (°C)	Time (hrs.)	Initial pr. (mbar)	Working pr. (mbar)	Bias voltage (V)	N_2:H_2
CrMoV	450;550	10	0.06×10^{-2}	~ 0.5	-250	4:1

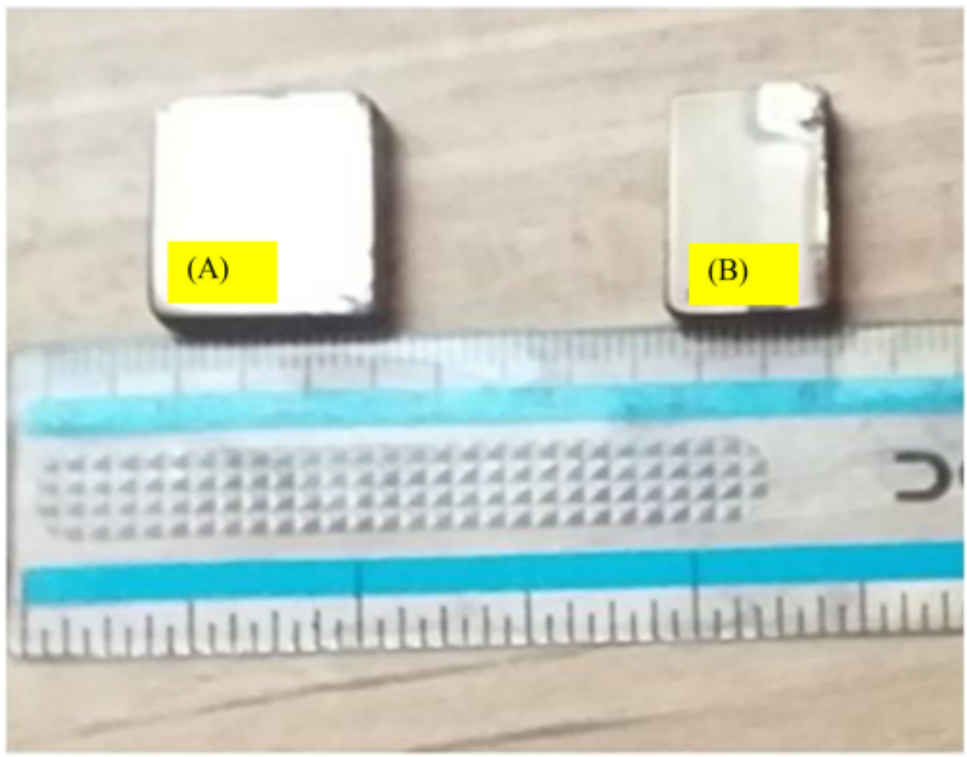

Fig. 1 Surface appearance of the bare steel A and the nitrided steel B

the nitrided steels. XRD was utilized for the phase evolution by using Co-$k\alpha$ radiation source (0.17902 nm). The cross-sectional analyses after metallographic polishing and etching with the Villela's reagent had been carried out under scanning electron microscope coupled with the energy dispersive spectroscopic analyses (SEM-Jeol, JSM5900).

To understand the mechanical properties bare and the nitrided steels were exposed to hardness measurements. Hardness was measured in terms of Vicker's microhardness by using LECO MST 210 microhardness tester at 50 g. applied load. The hardness was measured five times with the accuracy of $\pm$ 25 H_v and average values were finally taken and plotted the hardness depth profile.

After the structural characterization, sample coupons were exposed to the corrosion tests in 3.5 wt% NaCl environment. Linear sweep polarization tests were conducted by utilizing the corrosion testing instrument (Electrochemical Interface: Solatron Analytical, U.K. → Model S1 1287) interfaced to a personal computer with software to data acquisition and analyses. A three electrode cell was utilized for this purpose. The cell consisted of → (a) saturated calomel electrode through the Luggin probe used as the reference electrode for all the potential measurements; (b) steel coupons connected as the working electrode and; (c) a counter electrode → Pt. electrode. Before the tests, the electrolyte was purged with the nitrogen gas to create the inert environment. Polarization tests were carried out by following ASTM G59-97 (2914) standard test method.

The scanning rate of the polarization was fixed at 1 mV/s. Finally, the polarization diagrams were analyzed after Tafel's extrapolation and the corrosion parameters were calculated.

3 Results and Discussion

3.1 X-ray Diffraction (XRD) and Scanning Electron Microscopic (SEM) Analysis

All the nitrided and bare steels were exposed to detailed X-ray diffraction studies (using Co-k_a radiation source) for understanding the phase formation on the surface layer (shown in Fig. 2). XRD revealed α-Fe (110), (200) and (211) peaks in the bare steel. After nitriding Fe_xN nitrides (x = 2–3, 4) peaks appeared in CM45-10 and CM55-10 steels (Fig. 2b, c). Both these steels were nitrided for the same duration of 10 h but at the two different temperatures 450 °C and 550 °C respectively.

It is clear from the XRD patterns that peaks of ε-nitride (ε-$Fe_{2-3}N$) along with the γ'-nitride (Fe_4N) and CrN appear after nitriding. The presence of ε-nitride is known to improve the resistance to corrosion. From Fig. 2d, it is clearly indicated that there is major peak α-Fe shifting toward left side after nitriding of the steel at higher temperature of 550 °C. This may be attributed to the lattice strain. Careful observation shows that same is true for the nitriding at 450 °C. Broad view of these peaks and its position can be further represented by Fig. 3 as given below. A careful observation shows the lower angle shifting and peak broadening after nitriding of the steel.

By considering the full width at half maximum (FWHM) of α- Fe peaks of CM0 and CM55-10 steels, the peak broadening has been calculated to be ∼ 75%. This indicates that the lattice strain is developed as a result of nitrogen atom

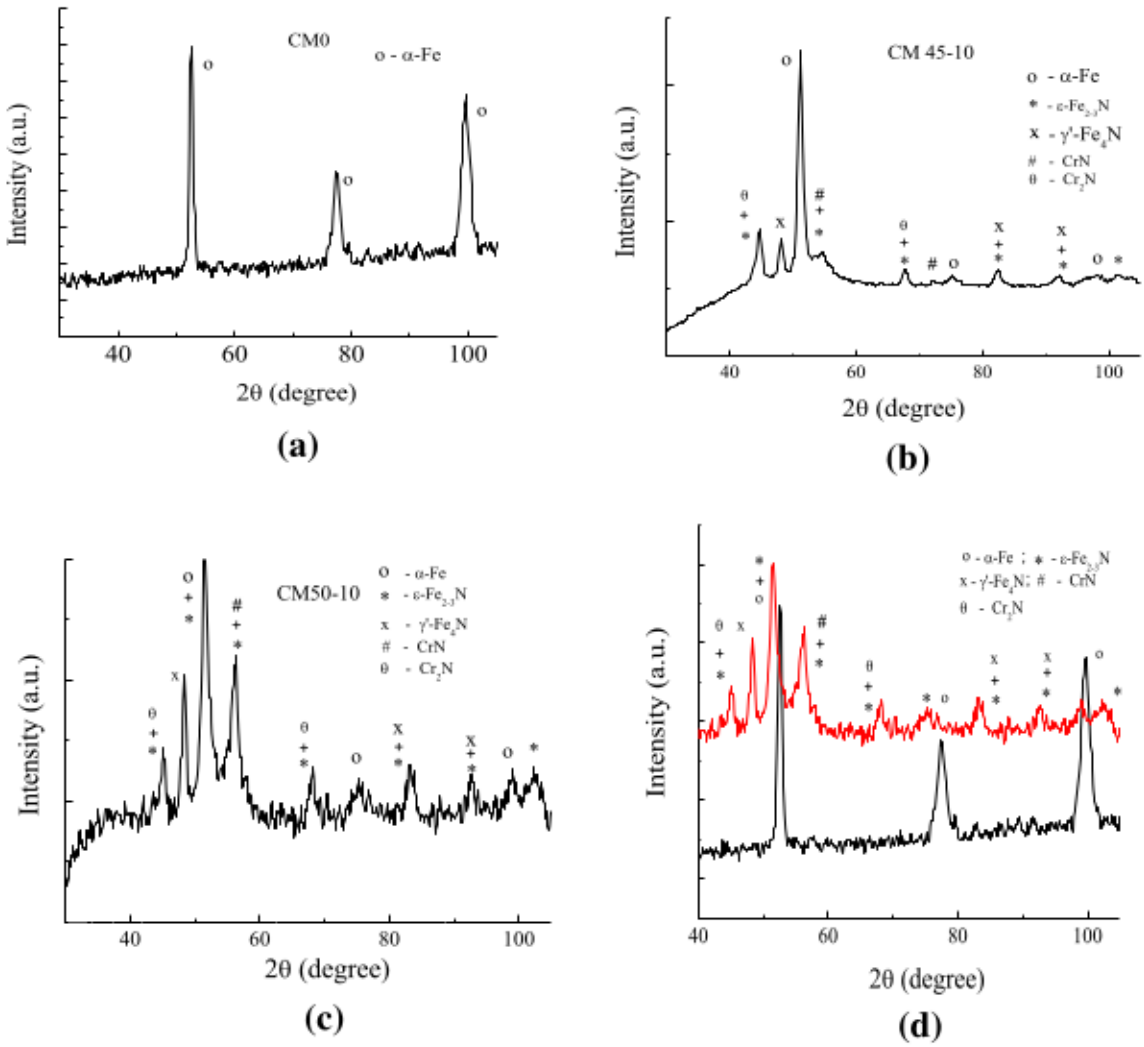

Fig. 2 Representation of X-ray diffraction patterns of: **a** CM0 (bare steel) **b** CM45-10; and **c** CM 55-10; **d** stacked (**a** and **c**; XRD patterns representing the peaks shifting after nitriding)

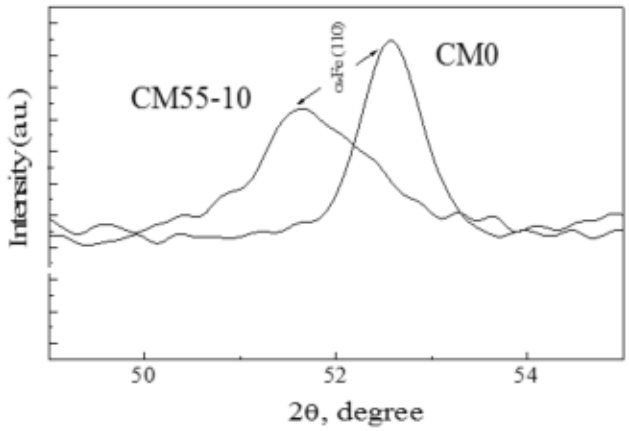

Fig. 3 α-Fe (110) peaks of the CM0 and the CM55-10 steels representing the lower angle peak shifting

dissolution and super saturation thus expanding and generating the compressive stress in the crystal lattice of the nitrided steel. Rise in hardness value and resistance to fatigue of the nitrided steel could be attributed to the supersaturation of nitrogen in the crystal interstices. The nitrogen incorporated will be released at the interface of surface and the electrolyte generating the NH_4^+ ions which in aqueous environment as NH_4OH make the electrolyte alkaline. The increased alkalinity of the electrolyte could be one of the reasons to disfavor the corrosion of steel.

On the other hand, the γ'- and ε- nitrides as revealed by XRD patterns are partially responsible for the improvement of corrosion resistance of the nitrided steel. When compared the peak intensities of these nitrides, the steel nitrided at the higher temperature of 550 °C (CM55-10) shows higher intensities. It can be speculated here that the CM55-10 steel has larger concentration of these nitrides. ε nitride as the predominating phase with higher concentration in this steel contributes more toward the resistance to corrosion.

Following XRD studies, both the nitrided steels CM45-10 and the CM55-10 were exposed to SEM/EDS analysis after metallographic polishing and etching with the Villela's reagent. The microstructure of the nitrided layer and the elemental availability across the cross section are revealed in this analysis. Point analysis was made from the top toward the bulk of the steel at 4 successive locations. Figure 4a, b as shown below represents the cross sectional microstructure along with the elemental analysis as captured by the SEM/EDS point analysis near the surface region. It is clear that the concentration of nitrogen at the surface is maximum and gradually decreases toward the core. A thin compound layer appeared at the top of the samples. Although, this layer is good from corrosion resistance point of view, but owing to its brittle nature, it may cause mechanical degradation.

Following the compound layer, a diffusion layer is formed which consists of Fe-nitrides, CrN and the nitrogen solid solution as clear from XRD analysis. Small precipitates may be the Fe-carbides. But further analysis is required for the confirmation. This layer contributes to the corrosion resistance of the steel. In Fig. 4c, the cross-sectional elemental analysis from top to the bulk of the steel reveals the presence of the alloying elements with variable concentration. Nitrogen availability is obvious from Fig. 4c. It clearly indicates that the nitrogen concentration at the top is maximum and gradually decreases toward the bulk of the steel.

3.2 Hardness Measurements

Hardness measurements of all the bare and the nitrided steel samples were carried out in terms of Vickr's microhardness tests. The tests were performed to understand the modification in mechanical properties of nitrided steels. The hardness *vs.* depth profiles are represented in the following Figs. 4a, b and 5. Figure 4a, b represent the SEM micrographs of the nitrided steels. The layers overlaid with the hardness vs. depth profile show the hardened layer's thickness/case depth. It is obvious from the curves as shown in this figure that the surface hardness attains a significantly high hardness value of around 1180 ± 30 H_v. The hardness of the bare steel is around 650 H_v. The hardness improvement is around two fold. These depth profiles explain the higher concentration of nitrogen and the nitride of Fe/Cr at the surface level and gradually decrease toward the core of the steel. For the steel nitrided at the lower temperature of 450 °C, the case depth is found to be ∼ 86 μm. and ∼ 153 μm for the steel nitrided at the higher temperature of 550 °C. A significantly wide case depth is obtained at the higher temperature nitriding. A wider case depth may prolong the longevity of the component in the harsh service conditions where the surface faces frequent frictional forces. Plasma nitriding thus proves to be beneficial for the wood machining steel by producing the protective layer and thus improving the service life of the tools.

3.3 Electrochemical Characterization

Potential Versus Time Analyses Both the bare and the nitrided steel samples were immersed into the cell containing the electrolyte 3.5 wt% NaCl and left for 1 h. until the voltage fluctuations subsided. Voltage vs. time plots for the three steels → (a) CM 0 (bare steel); (b) CM 45–10 (nitrided at 450 °C for 10 h); (c) CM 55–10 (nitrided at 550 °C for 10 h) were recorded and presented in the following Fig. 6a → c.

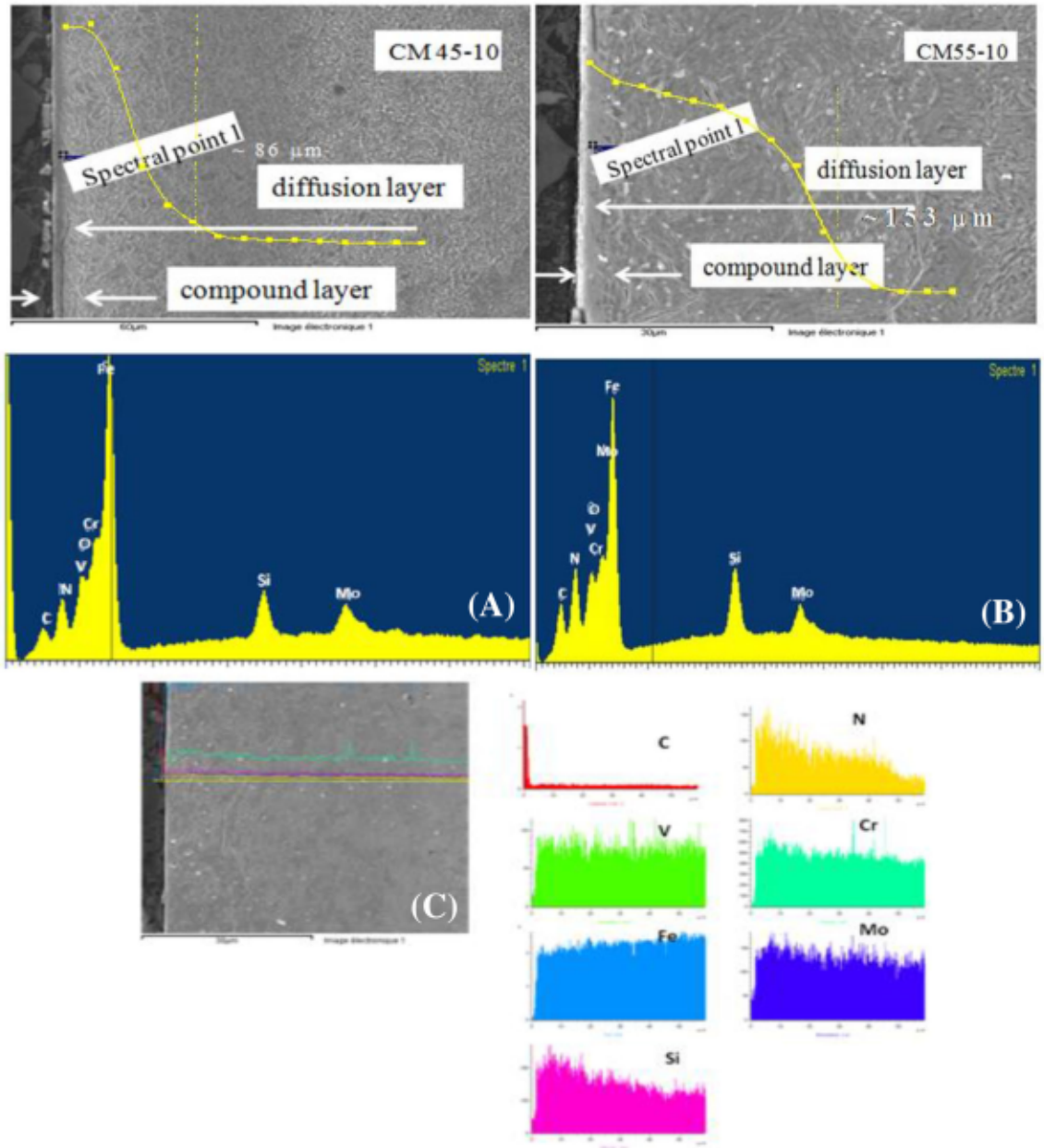

Fig. 4 SEM coupled with EDS across the cross section of the **a** CM45-10 steel; **b** CM55-10 after etching with Villela's reagent (×1000) and **c** elemental analysis across the cross section of CM55-10

The above diagrams reveal the three stages → (a) initial stage from where the potential rises sharply; (b) maximum potential region; (c) the final and the stable potential region indicating the gain of stability. Table 3 summarizes the potential variations in the three stages of bare and nitrided steels.

From Fig. 6a, it is revealed that the bare steel CM0 initially has most active potential – 0.64 V ($E_{initial}$) and the maximum potential of − 0.31 V which is more positive potential/noble potential. Then, the potential falls to − 0.51 V stable potential. This may be attributed to the surface flaw/defects causing the dissolution of the steel in the initial stages. XRD shows the formation of CrN and Fe_xN which may lead to the surface heterogeneity. It may also be speculated that the lower temperature nitriding may provide the scope to grow these precipitates as the nitrogen diffusion is slower in this case. These precipitates may form the microgalvanic cells on the surface which causes the faster dissolution.

The retention time at this maximum potential (− 0.31 V) is of few moments only and then fall down to − 0.51 V and subsequently attains stability at this

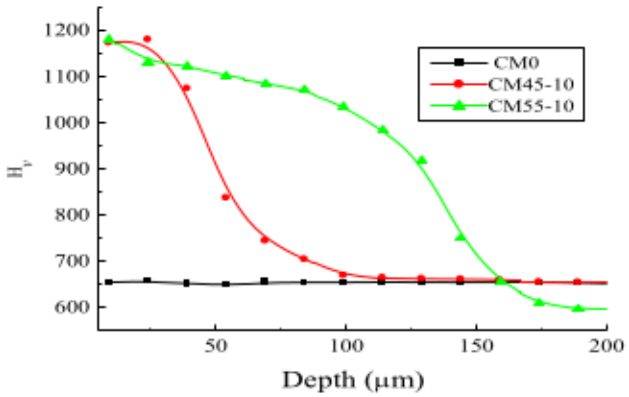

Fig. 5 Hardness vs. depth profiles of steels after plasma nitriding at low and high temperatures

potential. More positive value in comparison to the initial value may be due to the formation of passive film.

After nitriding of steel at low temperature of 450 °C, the initial potential—0.56 V is reached, which is more noble than that shown by the steel CM0 (Fig. 6b). Then the peak potential of − 0.38 V is attained which immediately falls to − 0.49 V stable potential. However, the difference of this potential is marginal when compared to that of the bare steel CM0.

CM 55–10 steel (Fig. 6c) has shown the lesser propensities toward the corrosion as compared to the bare and the CM 45–10 nitrided steels. Initial potential and also the maximum potential is – 0.58 V, which is lesser than that shown by the bare steel (− 0.64 V) and almost similar to that of the value shown by the C45-10 steel. However, the stability gained is at the higher potential of − 0.40 V, which is more positive than the other steels. It could be due to the fact that release of nitrogen is more in the nitrided steels, which makes the environment more alkaline and thus favor the resistance to corrosion. After achieving the

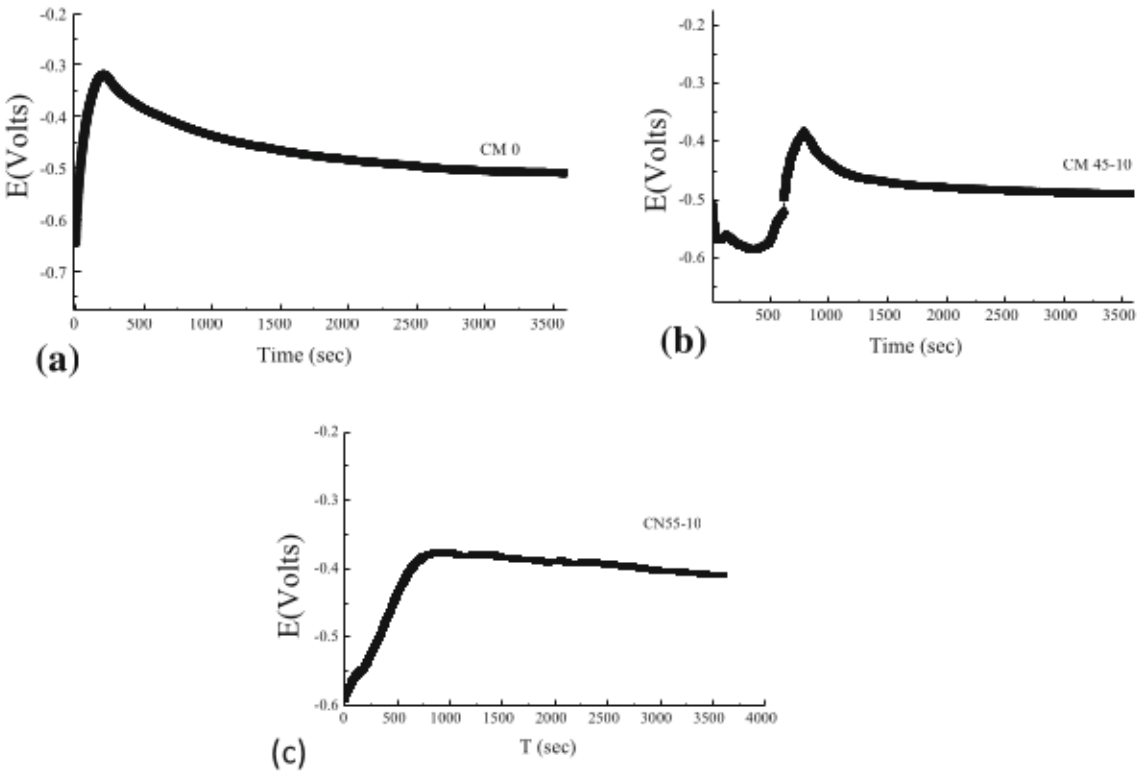

Fig. 6 Potential versus time curves of → **a** bare steel and the nitrided **b** CM45-10 and **c** CM55-10 steels

Table 3 Variation of potential with time of immersion of steels before and after nitriding in the 3.5 wt% NaCl electrolyte

Sample code	$E_{maximum}$ (V)	E_{stable} (V)	$E_{initial}$ (V)
CN0	− 0.31	− 0.51	− 0.64
CN45-10	− 0.38	− 0.49	− 0.56
CM 55-10	− 0.37	− 0.40	− 0.58

stability, these steels are exposed to the potentiodynamic polarization.

Potentiodynamic Polarization Tests All the bare and nitrided steels were exposed to the potentiodynamic polarization tests. After purging with the nitrogen, polarization was carried out in 3.5 wt% NaCl in the scan range ± 1.0 V and rate 1.0 mV/s. The bare steel CN0 shows the E_{corr} value − 0.4958 V, whereas the nitrided steel CN45-10 shows − 0.663 V. However, the E_{corr} for the CM55-10 steel has shown this value to be equal to − 0.562 V which is nobler than that of CM45-10 showing − 0.663 V. This is slightly less noble than the bare steel. Thus, the CM55-10 steel has shown the corrosion propensity less than shown by the CM45-10 steel. The polarization curves are represented in Fig. 7 a, b.

After Tafel extrapolation on the polarization curves, the corrosion parameters have been calculated and summarized in Table 4.

It seems that the bare steel had lesser flaws/defects on the surface as compared to that of the nitrided steels which

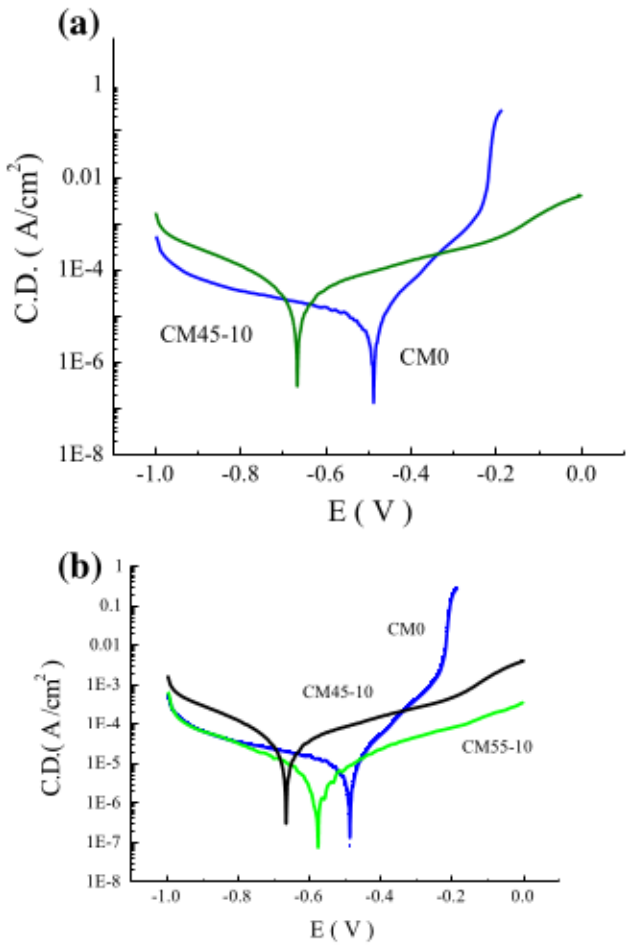

Fig. 7 Potentiodynamic polarization diagrams of steels **a** CM0 and CM45-10; **b** CM0, CM45-10 and CM55-10 steels; showing a distinct passivity and lower current density for the nitrided steels.

may be the reason of its nobler potential. The possibility that the nitrided steels may have the Fe-nitrided precipitates which may have created the surface heterogeneity.

On the other hand, comparison of the i_{corr} values for these steels, shows the order: I_{corr} (Amp/cm^2) values observed for these steels can be represented in the increasing order as $2.646 \times 10^{-6} < 8.678 \times 10^{-6} < 1.816 \times 10^{-5}$, respectively, for the steels as CM55-10 < CM0 < CM45-10. Thus, the dissolution kinetics of CM55-10 steel has been found to be lesser than the other steels. Similar is the case with the rate of corrosion where the order of rate of corrosion (MPY) can be given as: $1.085 < 3.659 < 7.660$ and accordingly the order of the steels in terms of rate of corrosion can be given as CM55-10 < CM0 < CM45-10. Therefore, it may be concluded that the corrosion resistance of CM55-10 steel is more than other steels. The resistance to corrosion for this steel is significantly higher than the CM45-10 steel. It may be suggested here that nitriding at the higher temperature is more effective to incorporate more nitrogen into the steel which makes the solution more alkaline in the electrolyte and thus causing more resistance to the corrosion.

From the XRD, it is clear that the ε-$Fe_{(2-3)}$ N peaks obtained after 550 °C nitriding have higher intensity than that obtained after 450 °C nitriding. If we look for the peaks from left to right direction, the peaks representing ε-$Fe_{(2-3)}$ N in steel nitrided at higher temperature have higher intensity. It is also known that ε-$Fe_{(2-3)}$ N formation increases with the rise in temperature. It is known that ε-$Fe_{(2-3)}$ N possess good corrosion resistance. CrN precipitation is common in both the nitrided steels, in fact formation of CrN is favored at 450 °C and with the rise in temperature, the precipitation of this phase is more. It may be suggested here that the overall concentration of ε-$Fe_{(2-3)}$ N and nitrogen in the solid solution is more than that found after nitriding of the steel at the lower temperature of 450 °C. Hence, the corrosion resistance is better in the steel nitrided at the higher temperature of 550 °C.

The bare steel may be showing better corrosion resistance initially, but later the corrosion kinetics is faster than that of the 450 °C nitrided steel. Maybe because of the FexN phase formation and its dispersion affects the surface homogeneity. Presence of CrN phase after nitriding, as evidenced by the XRD analysis obviously will cause the deterioration of the corrosion resistance because of the Cr depletion from the solid solution. In the bare steel, there is no Cr depletion and CrN phase formation which could be the reason of better corrosion resistance than the nitrided steel at this lower temperature. However, further studies will be focused on the concentration of various nitrides and CrN phase dispersed on the surface layer. It seems that after the dissolution of the first few surface layers, the lower layer get exposed which consists of the nitrogen

Table 4 Corrosion parameters obtained after Tafel extrapolation on polarization curves

Steel code	Corrosion rate (MPY)	Corrosion current (i_{corr} in Amp/cm^2)	Corrosion potential (E_{corr} in Volts)
CM0	3.660	8.678×10^{-6}	− 0.496
CM45-10	7.660	1.816×10^{-5}	− 0.663
CM55-10	1.085	2.646×10^{-6}	− 0.575

incorporated and the FexN (where, x = 2–3, 4) layer with less CrN or less Cr depleted layer. So, a better passivation range and lower dissolution kinetics is shown by the nitrided steel in comparison to that of the bare steel (Fig. 3a).

Feng et al. [37] worked on the role of nitrogen on microstructure, passivity and corrosion resistance of martensitic stainless steel. It has been suggested in this study that the inclusion of nitrogen in the martensitic stainless steel reduces the concentration of $M_{23}C_6$ content and converts to the precipitates of M_2N which improves the resistance to corrosion. However, high concentration of M_2N phase is detrimental form the corrosion resistance point of view. The change in microstructure first increases and then deteriorates the corrosion resistance with the increase of nitrogen.

Nitrogen incorporation which increases the Cr concentration as Cr_2O_3 and CrN in the passive layer and also the formation NH_4^+ ions improves the protective ability. It has also been suggested that the increase in nitrogen concentration in the solid solution increases the repassivation ability [37]. These reasons could be attributed to the improvement of corrosion resistance with the increase of process temperature and hence increase in nitrogen inclusions.

From the above results it can be concluded that plasma nitriding at the higher temperature of 550 °C has shown a significant improvement in hardness and corrosion resistance the CrMoV steel. These improvement may be attributed to the presence of FexN (where x = 2–3, 4) and CrN phases along with the nitrogen solid solution.

4 Conclusions

In the present work, it has been shown that the nitrogen inclusion by following plasma nitriding at a higher temperature of 550 °C for 10 h is effective for the improvement of hardness and corrosion resistance. Improvement in corrosion resistance after nitriding at the lower temperature of 450 °C is not so effective as in the case of higher temperature nitriding. It could be due to the nitrogen ingress in the solid solution at the higher temperature is greater owing to its greater rate of diffusion and also due to the presence of ε-$Fe_{2-3}N$ phase. It may also be suggested here that the higher nitrogen concentration renders the environment more alkaline and thus disfavor the corrosion of the steel.

Chromium–molybdenum–vanadium based alloy steel may be nitrided at the higher temperature of 550 °C for the improvement of both hardness and corrosion resistance. Nitriding at this temperature prolong the longevity of wood machining CrMoV tool steel in the harsh service conditions. Hence, the early replacement of the tools can be avoided and thus the cost of materials and manufacturing can be minimized.

Acknowledgements Authors are thankful to GITAM (Deemed to be University) for the encouragements to perform and publish this work. Experimental support from ENSAM, Paris Institute of Technology, France is thankfully acknowledged.

References

1. Valentin G, and Gavriljuk H B, *High Nitrogen Steels: Structure, Properties, Manufacture, Applications*, Springer, Berlin (1999).
2. Li H B, Zhou E Z, Ren Y B, Zhang D W, Xu D K, Yang C G, Feng H, Jiang Z H, Li X G, Gu T Y, and Yang K, *Corros. Sci.* **111** (2016) 811.
3. Li H B, Jiang Z H, Feng H, Zhang S C, Li L, Han P D, Misra R D K, and Li J Z, *Mater. Des.* **84** (2015) 291.
4. Gavriljuk V G, and Bems H, *High Nitrogen Steels: Structure, Properties, Manufacture, Applications*, Springer, Berlin (1999).
5. Mudali U K, and Raj B, *High Nitrogen Steels and Stainless Steels*, ASM International, (2004) p 133.
6. Sagar M, Katada Y, and Kodama T, *ISIJ Int.*, **43** (2003) 714.
7. Park J W, Shankar Rao V, and Kwon H S, *Corrosion*, **60** (2004) 1009.
8. Mudali U K, Khatak H S, Raj B, and Uhlemann M, *Mater. Manuf. Process*, **19** (2004) 61.
9. Khoshnaw F M, Kheder A I, and Ali F S M, *Anti Corros. Methods Mater.*, **54** (2007) 173.
10. De Anna L, Cerisola G, Bonora P L, Russo S L, Sootoni PM, and Tosello C, *Mater. Corros.* **31** (2004) 783.
11. Srikanth S, Sarwanan P, Joseph A, and Ravi K, *J. of Mater. Engg. Perf.*, **22** (2013) 2610.
12. Agren J, *Metall. Trans. A*, **10** (1979) 1847.
13. Hillert M, and Jarl M, *Metall. Tras. A*, **6** (1975) 553.
14. Bell T, and Owen W S, *J. Iron Steel Inst.* **205** (1967) 428.
15. Kunze J, *Steel Res.* **57** (1986) 361.
16. Fu Y, Wu X Q, Han E H, Ke W, Yang K, and Jiang Z H, *Electrochim. Acta*, **54** (2009) 4005.
17. Jargelius Peterson R F A, *Corros. Sc.* **41** (1999) 1639.
18. Lei M K, Zhu X M, *J. Electrochem. Soc.* **152** (2005) B291.

19. Ningshen S, Kamachi Mudali U, Mittal V K, Khatak H S, *Corros. Sci.* **49** (2007) 481.
20. Lothongkum G, Wongpanya P, Morito S, Furuhara T, and Maki T, *Corros Sci.* **48** (2006) 137.
21. Baba H, Kodama T, and Katada Y, *Corros. Sci.* **44** (2002) 2393.
22. Park J W, Shankar Rao V, and Kwon H S, *Corrosion*, **60** (2004) 1099.
23. Levey P R, and van Bennekom A, *Corrosion*, **51** (1995) 911.
24. Ha H Y, Jang H J, Kwon H S, and Kim S J, *Corros. Sci.* **51** (2009) 48.
25. Qui X, Mao H, and Yang Y, *Corros. Sci.* **120** (2017) 90.
26. Ma X P, Wang L J, Quin B, Liu C M, and Subramanian S V, *Mater. Des.* **34** (2012) 74.
27. Nouveau C, Steyer P, Ram Mohan Rao K, and Lagadrillere D, *Surf. Coat. Technol.* **205** (2011) 4514.
28. Cherng Wen D, *App. Surf. Sci.* **256** (2009) 797.
29. Ram Mohan Rao K, Nouveau C, and Trinadh K, *Mat. Tod. Proc.*, **17** (2019) 26.
30. Wang L, Li Y, and Wu X, *Appl. Surf. Sci.* **254** (2008) 6595.
31. Maniee A, Mahboubi F, Soleimani R, *Mater. Des.* **60** (2014) 599.
32. O'Brien J, and Goodman D M, *Plasma (Ion) Nitriding, Metals Handbook*, American Society for Metals, Metals Park, OH vol 4 (1991) p 420.
33. Ram Mohan Rao K, Nouveau C, Khanna AS, Aneja KS, Trinadh K, *Mater. Tod. Proc.* **24** (2019) 1006–1010.
34. Forati Rad H, Amadeh A, and Moradi H, *Mater. Des.* **32** (2011) 2635.
35. Mashreghi A, Soleimani S, and Saberifar S, *Mater. Des.* **46** (2013) 2635.
36. Muñoz Riofano R M, Castteleti L C, Canale L C F, and Totten G E, *Wear* **265** (2008) 57.
37. Feng H, Jiang Z, Li H, Lu P, Zhang S, Zhu H, Zhang B, Zhang T, Xu D, and Chen Z, **144** (2018) 288.